CLINICAL VIGNETTES

Phenotypic Spectrum of *HCN4* Mutations
A Clinical Case

The hyperpolarization-activated cyclic nucleotide-gated (HCN) cation (Na+/K+) currents (If/Ih) are generated by 4 members of the channel family (HCN1–4).[1] These currents contribute to the pacemaker function[2] in heart and brain.[3] The HCN4 current is known to play a crucial role in the automaticity of the sinus node through the generation of a slow diastolic depolarization during the phase 4 of the cardiac action potential.[4] Thus, it is a crucial channel for appropriate pacemaker activity and conduction system function because it facilitates rapid repolarization. Interestingly, *HCN4* has been shown to be expressed in essentially the entire heart tissue.[5] Mutations in *HCN4* have been associated mainly with sick sinus syndrome phenotype[6]; however, in recent years, a broad spectrum of phenotypes has been reported, including sinus bradycardia,[7] inappropriate sinus tachycardia,[8] early-onset atrial fibrillation,[9,10] atrioventricular block,[11,12] idiopathic ventricular tachycardia,[13] left ventricular noncompaction (LVNC),[14–17] dilation of the aorta, and mood and anxiety disorders.[19] In the present study, we report a case with sick sinus syndrome, LVNC, mood and anxiety disorders, and ventricular fibrillation (VF) hosting 2 novel *HCN4*-pore mutations.

CASE REPORT

The index patient was a 36-year-old man, who presented initially with mood and anxiety disorders characterized by important depressive episodes. Previous clinical records revealed a slightly impaired left ventricular function, paroxysmal atrial fibrillation, frequent premature ventricular complexes, and nonsustained tachycardia originating from the right ventricle. Therapy with β-blocker was initiated but discontinued shortly because of profound sinus bradycardia, which did not resume after washout. A cardiac magnetic resonance imaging excluded a right ventricular cardiomyopathy. The left ventricle showed an uncommon hypertrabeculation; however, the criteria for an LVNC were not fulfilled at that time.

Eight years later, the patient was hospitalized because of heart failure and rapid conducted atrial fibrillation. At this time, he exhibited a severely depressed left ventricular function with left ventricular end-diastolic diameter of 62 mm, reduced right ventricular function (tricuspid annular plane systolic excursion of 8 mm) and biventricular apical hypertrabeculation more pronounced in the left side. With a β-blocker and amiodarone, spontaneous conversion to sinus rhythm occurred, but marked sinus bradycardia was noted, despite reduction of β-blocker and amiodarone doses (Figure 1A). While hospitalized, he presented frequent premature ventricular complexes and VF with the need of resuscitation (Figure 1B).

Reversible causes for VF were excluded, the resting electrocardiogram exhibited sinus bradycardia and left anterior fascicular block (Figure 1C). The echocardiography after recompensation of heart failure was diagnostic for LVNC[20,21] and showed an improved biventricular function (Figure 1D). A dual-chamber internal cardioverter defibrillator was implanted, and a dual chamber with rate response stimulation at

Helge Servatius, MD
Alessandro Porro, BS
Stephan A. Pless, PhD
André Schaller, PhD
Babken Asatryan, MD
Hildegard Tanner, MD
Stefano F. de Marchi, MD
Laurent Roten, MD
Jens Seiler, MD
Andreas Haeberlin, MD, PhD
Samuel H. Baldinger, MD
Fabian Noti, MD
Anna Lam, MD
Juerg Fuhrer, MD
Anna Moroni, PhD
Argelia Medeiros-Domingo, MD, PhD

Correspondence to: Argelia Medeiros-Domingo, MD, PhD, Department of Cardiology, Inselspital, Bern University Hospital, 3010 Bern, Switzerland. E-mail argelia.medeiros@insel.ch
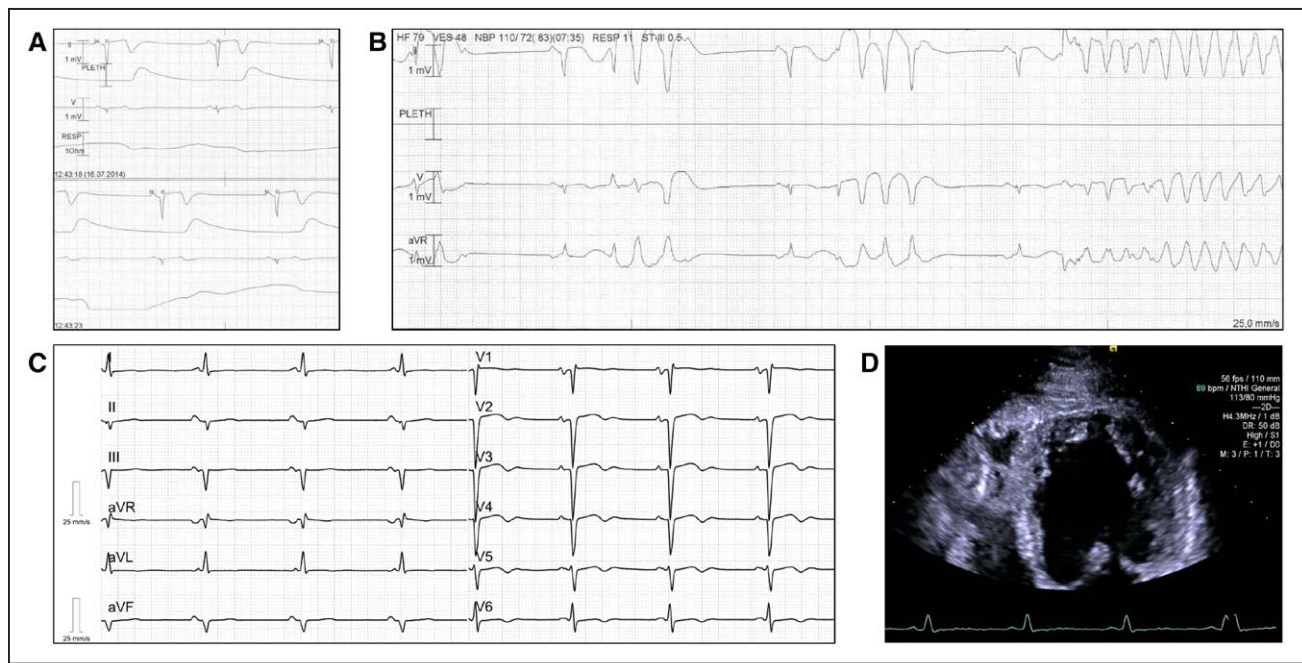
Figure 1. Electrocardiogram and echocardiographic characteristics of the proband.
A, Persistent sinus bradycardia after conversion from atrial fibrillation, despite low dose of β-blocker. **Top** to **Bottom**, simultaneous recording of ECG lead II, oxygen saturation wave, ECG lead V_1, and respiratory wave. **B**, Premature ventricular complexes triggering nonsustained ventricular tachycardia, followed by ventricular fibrillation with the need of resuscitation and external defibrillation (not shown). **Top** to **Bottom**, simultaneous recording of ECG lead II, PLETH (plethysmograph, oxygen saturation wave, disconected), ECG lead V_1, and ECG lead aVR. **C**, 12-lead ECG at rest, showing sinus bradycardia, left anterior fascicular block, and isodifasic T waves from V_2 through V_6. **D**, Four-chamber view echocardiogram after heart failure recompensation consistent with the diagnosis of left ventricular noncompaction cardiomyopathy (1. thickened myocardium with a noncompacted inner layer and compacted outer layer; 2. thickness ratio of noncompacted-to-compacted myocardium, >2; 3. typical predominant localization apical, midlateral, and midinferior[21]; and 4. thickness of the compacted myocardium, <8.1 mm).[20] ECG indicates electrocardiogram.

90 beats per minute with a long atrio-ventricular delay to avoid ventricular stimulation successfully prevented further ventricular arrhythmias. After 2 months, the stimulation rate was reduced to 70 beats per minute.

The patient's arrhythmic and LVNC phenotype at relatively young age raised a suspicion for a possible underlying inherited arrhythmogenic condition; therefore, genetic testing and familial evaluation were recommended. Because of patient's limited contact with all first-degree relatives, cardiac evaluation was only possible in 1 brother who was asymptomatic. The mother had a pacemaker implanted at 47 years of age and died 15 years later because of coronary heart disease; no tissue was available. The father died at 86 years of age, from an unknown cause.

METHODS

Subjects

The data, analytic methods, and study materials will not be made available to other researchers for purposes of reproducing the results or replicating the procedure because of patient confidentiality policy.

This study was conducted in full agreement with the principles of the Declaration of Helsinki and laws and regulations of Switzerland. All DNA donors available for this study signed an informed consent form approved by the local ethical committee.

Molecular Genetic Analysis

DNA was extracted from peripheral blood using standard procedures. Candidate gene sequencing was performed using the TruSight One Sequencing Panel (Illumina, San Diego, CA), containing 4813 genes associated with known clinical phenotypes. One hundred ninety-three genes previously associated with cardiac diseases were analyzed. Read alignment and local realignment of indels were performed using CLC Workbench v7.5.1 (Qiagen, Redwood City, CA). We used a number of different databases (HGMD Professional; Qiagen, Redwood City, CA) and published original literature to identify known disease-causing mutations in the datasets from the patients. Novel, putative disease-associated sequence variants were distinguished from polymorphisms using the following filtering criteria: a change in the protein's primary structure, species conservation of the underlying amino acid, and an allele frequency <1% based on the 1000 Genome Project database. For detailed sequence analysis and interpretation of sequence variations, we used the following bioinformatic algorithms and

databases: Polyphen2,[22] the Sorting Tolerant From Intolerant' (SIFT) algorithm,[23] Mutation Taster,[24] Human Gene Mutation Database (HGMD Biobase; Qiagen, Redwood City, CA), 1000 Genomes,[25] and the Exome Aggregation Consortium browser.[26] For titin protein, encoded by *TTN*, we considered as putative mutations only radical mutations (ie, nonsense, frameshift, and splice-site mutations). Final interpretation of variants was performed following the guidelines established by the American College of Medical Genetics and Genomics.[27]

Functional Assay

Human embryonic kidney (HEK)-293 cells were cultured in Dulbecco modified Eagle medium (Euroclone, Milan, and Italy) supplemented with 10% fetal bovine serum (Euroclone, Milan, and Italy), 1% Pen Strep (100 U/mL of penicillin and 100 µg/mL of streptomycin), and stored in a 37°C humidified incubator with 5% CO_2. HEK-293 cells were transiently transfected with WT (wild type) or mutant human HCN4 cDNA (codon-optimized synthesis using the Gene Art service by Thermo Fisher Scientific, Waltham, MA) using Turbofect transfection reagent (Thermo Fisher, Waltham, MA) according to the manufacturer's recommended protocol. For each 35-mm Petri dish, 1 µg or 0.5 µg of the HCN4-containing vector (pcDNA3.1) and 0.3 µg of green fluorescent protein (GFP)-containing plasmid (pmaxGFP; AmaxaBiosystems, Gaithersburg, MD) were used. In heteromeric studies, the amount of each HCN4 plasmid was 0.5 µg per Petri dish. In the control cell, 1.3 µg of GFP-containing plasmid was used for the transfection. Thirty to 72 hours after the transfection, the cells were dispersed by trypsin treatment. Green fluorescent cells were selected for patch-clamp experiments at room temperature (≈25°C). Currents were recorded in whole cell configuration with a Dagan 3900A (Degan, Minneapolis, MN); data were digitized with an Axon Digidata 1322 A/D (Axon Instruments, CA) converter and analyzed off-line with Axon pClamp9. Patch pipettes were fabricated from 1.5 mm outer diameter borosilicate glass capillaries with a P-97 Flaming/Brown Micropipette Puller (Sutter, Novato, CA) and had resistances of 3 to 5 mol/LΩ. The pipettes were filled with a solution containing 10 mmol/L NaCl, 130 mmol/L KCl, 1 mmol/L EGTA, 0.5 mmol/L $MgCl_2$, 2 mmol/L ATP (mg salt), and 5 mmol/L HEPES–KOH buffer (pH 7.4). The extracellular bath solution contained 110 mmol/L NaCl, 30 mmol/L KCl, 1.8 mmol/L $CaCl_2$, 0.5 mmol/L $MgCl_2$, and 5 mmol/L HEPES–KOH buffer (pH 7.4).

For channel activation, hyperpolarizing steps (ranging from −160 to −25 mV) of variable duration, sufficient to reach steady-state activation at all voltages, were applied from a holding potential of −40 mV, and current tails were measured on return to a fixed voltage (−40 mV). Only cells in which a 1 GΩ seal or better was achieved were kept for analysis. No leak subtraction was used.

To analyze current density, the steady-state current amplitude was measured at the end of each test potential and normalized to cell capacitance. Mean activation curves were obtained by fitting maximal tail current amplitude, plotted against the voltage step applied, with the Boltzmann equation $I_t=I_t(max)/(1+exp(V−V_{1/2})/k)$ where I_t is the current amplitude of the tail current recorded for a given prepulse and $I_t(max)$ is the maximum current amplitude of the tail current,

V is the voltage of the prepulse, $V_{1/2}$ is the half-activation voltage, and k is the slope factor in mV using Originpro software (Originlab, Northampton, MA). Activation time constants were obtained by fitting with a single exponential function, $I=I_0exp(−t/\tau)$, to current activation time courses during the hyperpolarizing reported steps. All comparisons were made using unpaired Student *t* tests with Origin software. All data are presented as mean±SEM.

RESULTS

Two novel mutations in the *HCN4* gene were found in the proband: c.1454C>A p.(Ala485Glu) and c.1435A>G p.(Ile479Val). Both variants were present in the same Next Generation Sequencing reads suggesting that they were in cis c.(1454C>A; 1435A>G). They both localized to the pore region of the HCN4 channel and were predicted to be pathogenic by SIFT, Polyphen2, Mutation Taster, and were absent in HGMD, 1000 Genomes, and Exome Aggregation Consortium Browser encompassing >60 000 sequenced exomes. The patient's brother did not carry any of the 2 *HCN4* mutations. No tissue was available from the parents for genetic examination.

Transfected HEK-293 cells transiently expressing the WT and the mutant channels were subjected to electrophysiological measurements, example currents were obtained from cells transfected with 1 µg of HCN4 plasmid, whereas cells transfected with only GFP plasmid served as a control. (Figure 2A and 2B). WT channels produced the typical time- and voltage-dependent inward currents that result in the current/voltage relationship and activation curve (Figure 2C and 2D). By fitting the Boltzmann equation to the activation curve (Figure 2D), we obtained a half-activation value of −103.1±0.2 mV and a slope factor k=11±0.2 mV. These values are consistent with published data on HCN4[28] functionally expressed in HEK-293 cells. Notably, transfection of 1 µg of the single mutants (I479V and A485E), as well as of the double mutant (I479V/A485E), did not generate any measurable HCN4-like current (Figure 2A). The small current of these cells is indistinguishable from that of the control cells, transfected with GFP only (Figure 2A and current/voltage relationship in Figure 2C).

When the double mutant was cotransfected with the WT channel (0.5 µg each plasmid), cells exhibited typical HCN4-like currents (Figure 2B). A detailed analysis showed that the voltage dependence (Figure 2D) of these currents and their activation kinetics (Figure 2E) were identical to that of the WT channel expressed alone. Only the amplitude of these currents was reduced by a factor of 2 (Figure 2C), suggesting that the decrease in current level was solely reflecting the reduced amount of WT plasmid in these experiments. The finding that WT channels, when coexpressed with
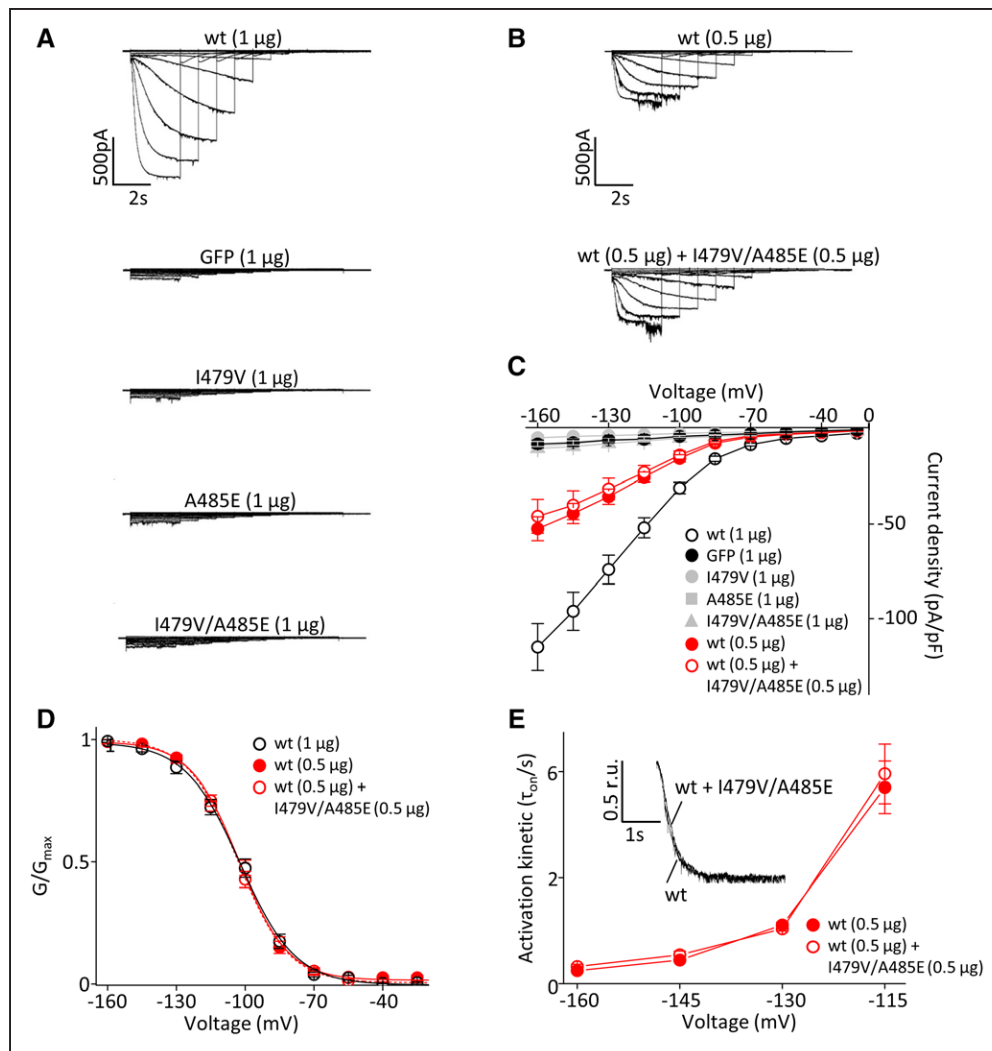
Figure 2. Functional expression of HCN4 WT (wild type) and mutant channels in HEK-293 cells.
A, Representative current traces recorded by patch clamp in cells transiently transfected with WT or mutant HCN4 channels (I479V, A485E, and I479V/A485E) using 1 µg of plasmid DNA; control cell was transfected with GFP. **B**, Currents recorded from cells transfected with WT channels (0.5 µg) or with a 1:1 mixture of WT and I479V/A485E channels (0.5 µg each). **C**, Mean steady-state current/voltage relationship (I/V) from cells transfected with 1 µg WT (open black circles), I479V (grey circles), A485E (grey square), I479V/A485E (grey triangles); 0.5 µg WT (open red circles), 0.5 µg WT+0.5 µg I479V/A485E (red circles); GFP (black circles). **D**, Mean activation curves of WT and WT+I479V/A485E currents (symbols as in [**C**]). Lines show data fits to a Boltzmann function yielding half-activation potential ($V_{1/2}$) and slope factor (k) values as follows $V_{1/2}=-103.1\pm0.2$ mV, k=11±0.2 mV; $V_{1/2}=-102.1\pm0.8$ mV, k=10.7±0.7 mV; $V_{1/2}=-102.6\pm0.9$ mV, k=12±0.8 mV for 1 µg WT, 0.5 µg WT, and 0.5 µg WT+0.5 µg I479V/A485E, respectively. **E**, Voltage dependency of activation time constant (τ_{on}) of WT and WT+I479V/A485E currents (symbols as in [**C**]). Inset shows exemplary current traces (recorded at −145 mV) from the 2 conditions superimposed after normalization. Number of cells: n=14 (1 µg WT); n=3 (GFP), n=5 (I479V); n=5 (A485E); n=14 (I479V/A485E); n=11 (0.5 µg WT); n=13 (0.5 µg WT+0.5 µg I479V/A485E). Number of cells in (**E**) was 9 for both conditions. r.u. indicates relative units.

the mutants, show WT-like currents underscores the notion that the mutants have no dominant-negative effect on functional channel.

DISCUSSION

HCN4 gene mutations were described initially in patients with sick sinus syndrome.[6] In recent years, it has become evident that additional phenotypes can be caused by mutations in *HCN4*. LVNC is one of the phenotypes described in recent years. In particular, the pore mutation p.Gly482Arg has been described several times in association with LVNC.[14,16] Here, we described another case with LVNC and 2 pore mutations in cis, close to the well-known *HCN4*-Gly482Arg mutation. We, therefore, hypothesize that this region represents a hot spot for the LVNC phenotype. We also observed a VF phenotype, not described before in *HCN4* muta-

tions; however, this severe arrhythmia may be multifactorial in our case and potentially triggered by the slow heart rate in the setting of previous treatment with amiodarone. Despite the fact that this drug was stopped, amiodarone is known to have long half-life. An additional phenotype detected was the previously reported mood and anxiety disorder.[19]

Our functional studies revealed that the double mutation and each single mutation alone by themselves were not able to generate a measurable HCN4 current. When they were coexpressed with the WT channel—a situation that mimics a heterozygous condition—they induced no appreciable changes to the functional properties of the WT channel. The observation that the double mutant does not act in a dominant-negative manner on the WT protein indicates that the heterozygous patient presumably expressed only half the number of HCN4 channels, with only the WT allele contributing to the HCN4 current. This would result in a significant reduction in HCN4 current. This interpretation is consistent with the experimental results, in which the current density reflects the amount of WT plasmid used for transfection. Such a reduced current density in a patient can lead to haploinsufficiency—a condition already described for another HCN4 mutation, P257S—associated with early-onset atrial fibrillation.[9] The P257S mutation is found in the N-terminus of the HCN4 protein and results in a trafficking-defective protein that does not reach the plasma membrane. In our case, the double mutation I479V/A485E is located in the pore loop, between the S5 and S6 transmembrane helices that contain the highly conserved [478]CIGYG[482] selectivity filter sequence. Further analysis, which is beyond the scope of this work, is needed to examine whether the mutations analyzed in this study alter protein trafficking or protein stability. Interestingly, 2 other mutations in the selectivity filter of HCN4 (Y481H and G482R) have been previously associated with[14] LVNC.[14,17] In these cases, the mutations also caused a loss of function that was either because of a negative shift of the activation curve[14] or a lower number of channels in the membrane with a consequent reduction of HCN4 current density.[17]

CONCLUSIONS

HCN4 mutations confer diverse phenotypes, characterized by the previously described bradycardia, sick sinus syndrome, LVNC, mood and anxiety disorders, and susceptibility to VF as described here. Our study clearly suggests that the HCN4-I479V/A485E mutant phenotype can be explained by a lower number of active channels rather than altered current properties. Collectively, the data suggest that the mutation reflects the situation of a partial knockout of the HCN4 channel.

DISCLOSURES

None.

AFFILIATIONS

From the Department of Cardiology (H.S., B.A., H.T., S.F.d.M., L.R., J.S., A.H., S.H.B., F.N., A.L., J.F., A.M.-D.) and Division of Human Genetics, Department of Pediatrics (A.S.), Inselspital, Bern University Hospital, University of Bern, Switzerland; Artificial Organ Center for Biomedical Engineering Research, University of Bern, Switzerland (A.H.); Department of Biosciences, CNR IBF-Milano, Università degli Studi di Milano, Italy (A.P., A.M.); and Department of Drug Design and Pharmacology, Center for Biopharmaceuticals, University of Copenhagen, Denmark (S.A.P.).

FOOTNOTES

Circ Genom Precis Med is available at http://circgenetics.ahajournals.org.

REFERENCES

1. Altomare C, Terragni B, Brioschi C, Milanesi R, Pagliuca C, Viscomi C, et al. Heteromeric HCN1-HCN4 channels: a comparison with native pacemaker channels from the rabbit sinoatrial node. *J Physiol*. 2003;549(pt 2):347–359. doi: 10.1113/jphysiol.2002.027698.

2. Stieber J, Herrmann S, Feil S, Löster J, Feil R, Biel M, et al. The hyperpolarization-activated channel HCN4 is required for the generation of pacemaker action potentials in the embryonic heart. *Proc Natl Acad Sci USA*. 2003;100:15235–15240. doi: 10.1073/pnas.2434235100.

3. Ludwig A, Zong X, Jeglitsch M, Hofmann F, Biel M. A family of hyperpolarization-activated mammalian cation channels. *Nature*. 1998;393:587–591. doi: 10.1038/31255.

4. Ye B, Nerbonne JM. Proteolytic processing of HCN2 and co-assembly with HCN4 in the generation of cardiac pacemaker channels. *J Biol Chem*. 2009;284:25553–25559. doi: 10.1074/jbc.M109.007583.

5. Ueda K, Nakamura K, Hayashi T, Inagaki N, Takahashi M, Arimura T, et al. Functional characterization of a trafficking-defective HCN4 mutation, D553N, associated with cardiac arrhythmia. *J Biol Chem*. 2004;279:27194–27198. doi: 10.1074/jbc.M311953200.

6. Nof E, Luria D, Brass D, Marek D, Lahat H, Reznik-Wolf H, et al. Point mutation in the HCN4 cardiac ion channel pore affecting synthesis, trafficking, and functional expression is associated with familial asymptomatic sinus bradycardia. *Circulation*. 2007;116:463–470. doi: 10.1161/CIRCULATIONAHA.107.706887.

7. Laish-Farkash A, Glikson M, Brass D, Marek-Yagel D, Pras E, Dascal N, et al. A novel mutation in the HCN4 gene causes symptomatic sinus bradycardia in Moroccan Jews. *J Cardiovasc Electrophysiol*. 2010;21:1365–1372. doi: 10.1111/j.1540-8167.2010.01844.x.

8. Baruscotti M, Bucchi A, Milanesi R, Paina M, Barbuti A, Gnecchi-Ruscone T, et al. A gain-of-function mutation in the cardiac pacemaker HCN4 channel increasing cAMP sensitivity is associated with familial inappropriate sinus tachycardia. *Eur Heart J*. 2017;38:280–288. doi: 10.1093/eurheartj/ehv582.

9. Macri V, Mahida SN, Zhang ML, Sinner MF, Dolmatova EV, Tucker NR, et al. A novel trafficking-defective HCN4 mutation is associated with early-onset atrial fibrillation. *Heart Rhythm*. 2014;11:1055–1062. doi: 10.1016/j.hrthm.2014.03.002.

10. Duhme N, Schweizer PA, Thomas D, Becker R, Schröter J, Barends TR, et al. Altered HCN4 channel C-linker interaction is associated with familial tachycardia-bradycardia syndrome and atrial fibrillation. *Eur Heart J*. 2013;34:2768–2775. doi: 10.1093/eurheartj/ehs391.

11. Zhou J, Ding WG, Makiyama T, Miyamoto A, Matsumoto Y, Kimura H, et al. A novel HCN4 mutation, G1097W, is associated with atrioventricular block. *Circ J*. 2014;78:938–942.

12. Baruscotti M, Bucchi A, Viscomi C, Mandelli G, Consalez G, Gnecchi-Rusconi T, et al. Deep bradycardia and heart block caused by inducible cardiac-specific knockout of the pacemaker channel gene Hcn4. *Proc Natl Acad Sci USA*. 2011;108:1705–1710. doi: 10.1073/pnas.1010122108.

13. Ueda K, Hirano Y, Higashiuesato Y, Aizawa Y, Hayashi T, Inagaki N, et al. Role of HCN4 channel in preventing ventricular arrhythmia. *J Hum Genet*. 2009;54:115–121. doi: 10.1038/jhg.2008.16.

14. Milano A, Vermeer AM, Lodder EM, Barc J, Verkerk AO, Postma AV, et al. HCN4 mutations in multiple families with bradycardia and left ventricular noncompaction cardiomyopathy. *J Am Coll Cardiol*. 2014;64:745–756. doi: 10.1016/j.jacc.2014.05.045.

15. Millat G, Janin A, de Tauriac O, Roux A, Dauphin C. HCN4 mutation as a molecular explanation on patients with bradycardia and non-compaction cardiomyopathy. *Eur J Med Genet*. 2015;58:439–442. doi: 10.1016/j.ejmg.2015.06.004.

16. Ishikawa T, Ohno S, Murakami T, Yoshida K, Mishima H, Fukuoka T, et al. Sick sinus syndrome with HCN4 mutations shows early onset and frequent association with atrial fibrillation and left ventricular noncompaction. *Heart Rhythm*. 2017;14:717–724. doi: 10.1016/j.hrthm.2017.01.020.

17. Schweizer PA, Schröter J, Greiner S, Haas J, Yampolsky P, Mereles D, et al. The symptom complex of familial sinus node dysfunction and myocardial noncompaction is associated with mutations in the HCN4 channel. *J Am Coll Cardiol*. 2014;64:757–767. doi: 10.1016/j.jacc.2014.06.1155.

18. Vermeer AM, Lodder EM, Thomas D, Duijkers FA, Marcelis C, van Gorselen EO, et al. Dilation of the aorta ascendens forms part of the clinical spectrum of HCN4 mutations. *J Am Coll Cardiol*. 2016;67:2313–2315. doi: 10.1016/j.jacc.2016.01.086.

19. Kelmendi B, Holsbach-Beltrame M, McIntosh AM, Hilt L, George ED, Kitchen RR, et al. Association of polymorphisms in HCN4 with mood disorders and obsessive compulsive disorder. *Neurosci Lett*. 2011;496:195–199.

20. Gebhard C, Stähli BE, Greutmann M, Biaggi P, Jenni R, Tanner FC. Reduced left ventricular compacta thickness: a novel echocardiographic criterion for non-compaction cardiomyopathy. *J Am Soc Echocardiogr*. 2012;25:1050–1057. doi: 10.1016/j.echo.2012.07.003.

21. Jenni R, Oechslin E, Schneider J, Attenhofer Jost C, Kaufmann PA. Echocardiographic and pathoanatomical characteristics of isolated left ventricular non-compaction: a step towards classification as a distinct cardiomyopathy. *Heart*. 2001;86:666–671.

22. Adzhubei IA, Schmidt S, Peshkin L, Ramensky VE, Gerasimova A, Bork P, et al. A method and server for predicting damaging missense mutations. *Nat Methods*. 2010;7:248–249. doi: 10.1038/nmeth0410-248.

23. Kumar P, Henikoff S, Ng PC. Predicting the effects of coding non-synonymous variants on protein function using the SIFT algorithm. *Nat Protoc*. 2009;4:1073–1081. doi: 10.1038/nprot.2009.86.

24. Schwarz JM, Cooper DN, Schuelke M, Seelow D. MutationTaster2: mutation prediction for the deep-sequencing age. *Nat Methods*. 2014;11:361–362. doi: 10.1038/nmeth.2890.

25. Auton A, Brooks LD, Durbin RM, Garrison EP, Kang HM, Korbel JO, et al; 1000 Genomes Project Consortium. A global reference for human genetic variation. *Nature*. 2015;526:68–74. doi: 10.1038/nature15393.

26. Lek M, Karczewski KJ, Minikel EV, Samocha KE, Banks E, Fennell T, et al; Exome Aggregation Consortium. Analysis of protein-coding genetic variation in 60,706 humans. *Nature*. 2016;536:285–291. doi: 10.1038/nature19057.

27. Richards S, Aziz N, Bale S, Bick D, Das S, Gastier-Foster J, et al; ACMG Laboratory Quality Assurance Committee. Standards and guidelines for the interpretation of sequence variants: a joint consensus recommendation of the American College of Medical Genetics and Genomics and the Association for Molecular Pathology. *Genet Med*. 2015;17:405–424. doi: 10.1038/gim.2015.30.

28. Lolicato M, Bucchi A, Arrigoni C, Zucca S, Nardini M, Schroeder I, et al. Cyclic dinucleotides bind the C-linker of HCN4 to control channel cAMP responsiveness. *Nat Chem Biol*. 2014;10:457–462. doi: 10.1038/nchembio.1521.

Circulation
Genomic and Precision Medicine

American Heart Association®

Phenotypic Spectrum of *HCN4* Mutations: A Clinical Case

Helge Servatius, Alessandro Porro, Stephan A. Pless, André Schaller, Babken Asatryan,
Hildegard Tanner, Stefano F. de Marchi, Laurent Roten, Jens Seiler, Andreas Haeberlin, Samuel
H. Baldinger, Fabian Noti, Anna Lam, Juerg Fuhrer, Anna Moroni and Argelia
Medeiros-Domingo

The online version of this article, along with updated information and services, is located on the
World Wide Web at:

http://circgenetics.ahajournals.org/content/11/2/e002033